# Time-Frequency Polarization Analysis and Filtering

Robert Pinnegar*
Calgary Scientific Inc., Calgary, Alberta, Canada
pinnegar@ucalgary.ca

**Abstract**

With multicomponent signal analysis becoming more common in exploration geophysics, it is natural that we would like to develop new techniques for polarization analysis and polarization filtering. Most of the existing methods operate in the time domain only, or in the frequency domain only. This causes a problem if the seismic data contain multiple events that have different polarization properties. Time-domain methods often cannot deal with overlapping events that have different frequencies, and frequency-domain methods can be compromised if any particular frequency band contains events that occur at different times. Some more recent techniques, such as the windowed covariance matrix technique of Jurkevics [1], have attempted to address these problems, but most such methods have the disadvantage of noninvertibility which means that they cannot be used for filtering.

The method described in this abstract tracks the time changes in the polarization properties of a signal through use of time-frequency representations (TFRs). The method is easiest to understand if we start by thinking of the whole seismogram in terms of the Fourier transforms of its orthogonal components [2]. The Fourier decomposition of the signal's vertical component gives a superposition of time-dependent sinusoids, each having a unique frequency and behaving like a vertically-oriented, one-dimensional harmonic oscillator. When the radial and transverse components are similarly decomposed, each frequency then contains three orthogonal sinusoids, giving three-dimensional harmonic motion. The result is elliptical motion in 3-space at each frequency. Thus the total signal can be thought of as a superposition of ellipses, instead of a superposition of sinusoids.

The result is that the traditional Fourier amplitude and phase spectra can be supplanted by new Fourier spectra of the elements of these ellipses: the semimajor and semiminor axes of each ellipse; the strike and dip of each ellipse plane; the pitch of each major axis; and the phase of the particle motion at each frequency. In practice, these spectra are also given explicit time dependence, through use of a translating window. This helps to avoid the disadvantages of working entirely in the time domain, or the frequency domain, by combining information from both domains to produce a TFR. The windowed Fourier transform is not the only TFR that can be used for this purpose; some other examples are wavelet transforms, and the Stockwell transform [3] which is the TFR used by us. The Stockwell transform is similar to a windowed Fourier transform, but has the advantage of a wavelet-like, scalable window that provides multiresolution analysis.

The test data used here to give an example of the method is shown in Fig. 1. This is a segment of a three-component broadband seismogram of an M = 6.9 earthquake, recorded at a seismic station in Pembroke, Ontario. This segment was selected because it contains the Love and

Rayleigh phases, which have distinctive and very different polarization properties. Here, the different components of the trace give the radial (x), transverse (y), and vertical (z)

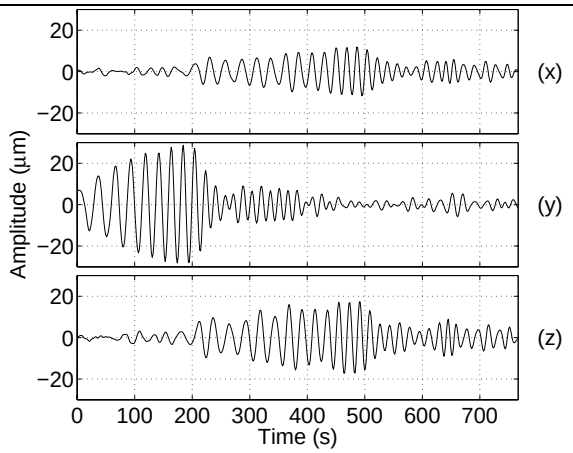


**Figure 1. Earthquake seismogram**

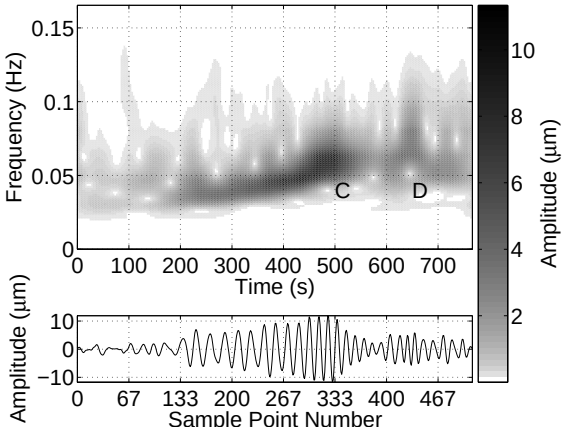


**Figure 2. TFR of radial component**

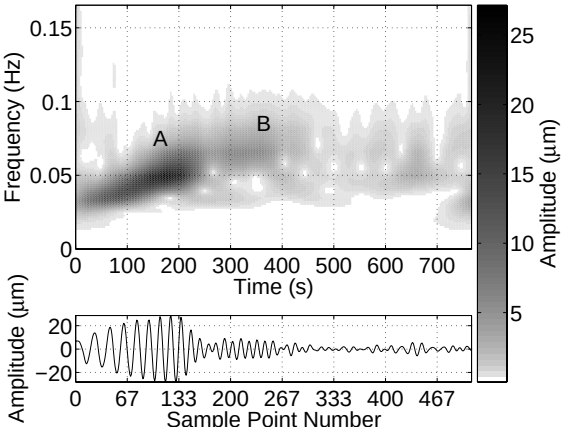


**Figure 3. TFR of transverse component**

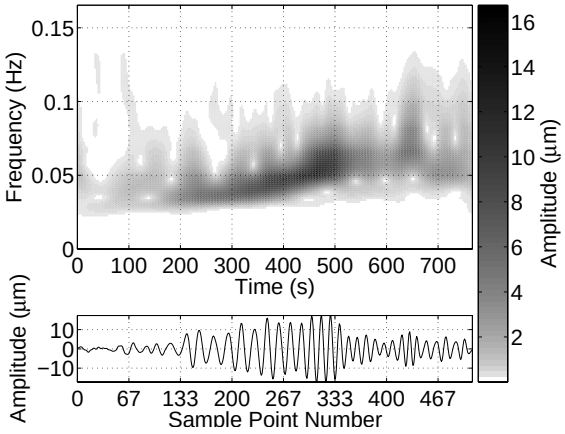


**Figure 4. TFR of vertical component**

components of the motion. The Stockwell amplitude spectra of the separate components appear in Figs. 2, 3 and 4. In Fig. 3, the first large amplitude event (marked A) is the Love wave arrival; in Figs. 2 and 4, the largest amplitudes (marked C on Fig. 2) are the Rayleigh wave arrival. (The lower amplitude events marked D and B on Figs. 2 and 3 have Love and Rayleigh properties respectively; these may represent higher-order phases, or, alternatively, crustal wave packets of relatively high frequency whose shallow penetration depths have delayed their arrival times.) Both the Love and Rayleigh waves show obvious dispersive effects, with the higher frequencies arriving later.

Figs. 5 and 6 show the Stockwell semimajor axis and semiminor axis spectra of the whole 3-component seismogram, obtained using the approach described above. In Fig. 6, the very low amplitude of the signature of the Love wave is a consequence of its nearly linear particle motion; the semiminor axis is nearly zero. The Rayleigh wave signature on Fig. 5 has about 1.5 times the

amplitude of the corresponding signature on Fig. 6, which indicates that the ratio of the major and minor axes of the Rayleigh ellipse is roughly 3:2. The Stockwell spectra of

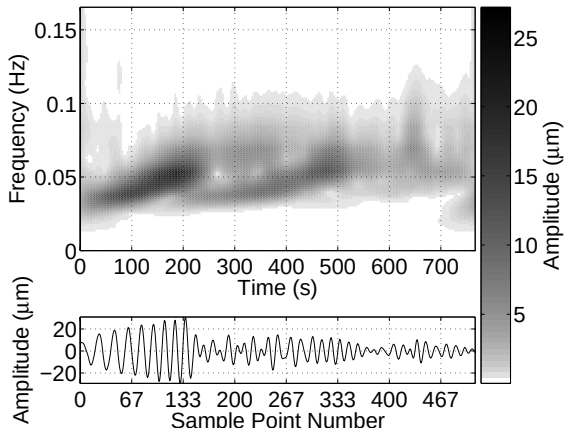


**Figure 5. TFR of semimajor axis**

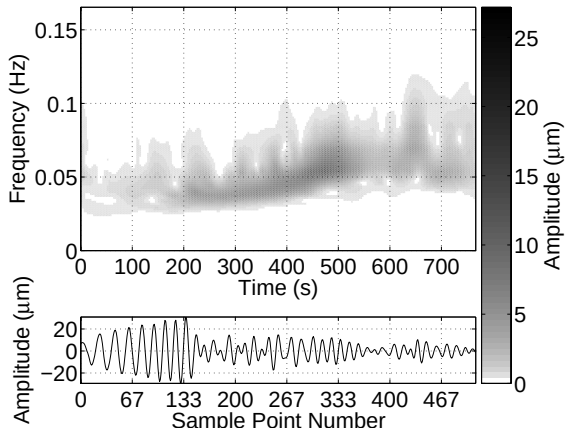


**Figure 6. TFR of semiminor axis**

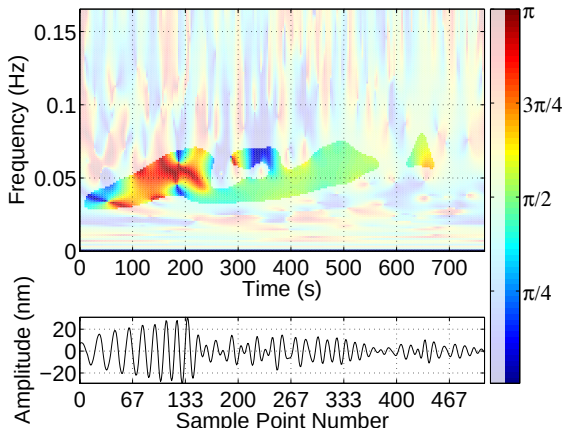


**Figure 7. TFR of ellipse plane dip**

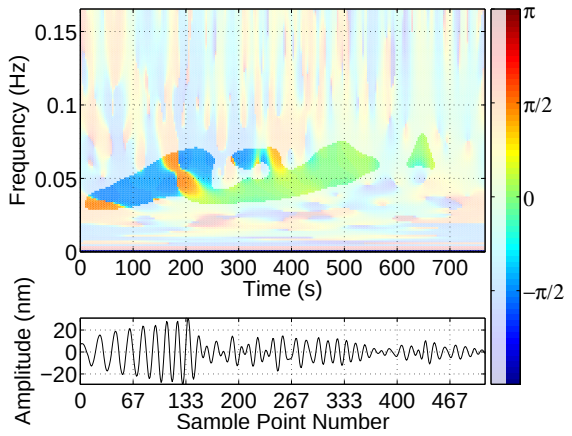


**Figure 8. TFR of ellipse plane strike**

the other elliptical elements can be difficult to interpret visually because, unlike Figs. 2- 6, they do not give any information about what parts of the time-frequency plane make the most significant contributions to the total signal. To this end, in Figs. 7 and 8, the values at each pixel are plotted using one of two different shades of the same colour. The brighter shades are used when the combined amplitude of Figs. 5 and 6 is larger than 7 μm. This cutoff value is useful for outlining the main Love and Rayleigh signatures. The Stockwell dip spectrum is shown in Fig. 7. Note that the Rayleigh wave signature has a dip of

$\sim\pi/2$, indicating a vertical ellipse plane as one would expect. On the Love wave signature, though, the dip is unstable. This happens because, for nearly-linear simple harmonic motion, even small noise contributions can lead to large changes in the dip of the ellipse plane (keep in mind that this is not the same as the plunge of the major axis).

The Stockwell strike spectrum of the Love wave, shown in Fig. 8, is more stable

and has a value of roughly $\pm \pi/2$ (the positive radial direction has a strike of 0 in this notation). This is not surprising since Love waves are transverse. The reason there are two possible values is that the "strike direction" is defined to be the azimuth that the particle has when it crosses the horizontal plane in the direction of increasing **z**. Thus, changing the strike by $\pm \pi$ is equivalent to reversing the direction of particle motion from counterclockwise to clockwise, here a result of

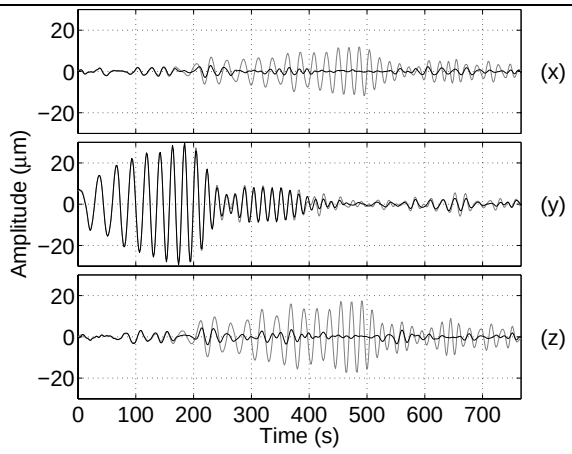


**Figure 9. Filtered seismogram**

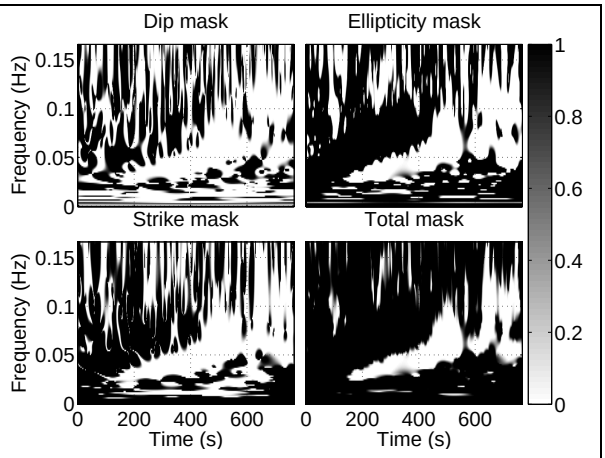


**Figure 10. Masking function**

noise contamination. (The need to specify the direction of motion also explains why some dip values are greater than $\pi/2$.) On the Rayleigh wave signature, the strike has a relatively stable value near 0, which tells us that the particle is displaced in the positive radial direction when it rises through the horizontal plane. This is consistent with the retrograde motion of the Rayleigh wave.

Like the Fourier transform, the Stockwell transform is invertible, and so these TFRs can be used to design signal-adaptive polarization filters to target parts of the signal that have specific polarization properties. Filters of this type are not restricted to reducing the whole amplitude of any particular ellipse, as would be the case for standard Fourier-domain filtering. Fig. 9 shows the data of Fig. 1 after the application of a filter that attacks the 3:2 Rayleigh wave, by reducing the semimajor axis by 3/2 times the semiminor axis, then setting the semiminor axis to zero. The filter is only active in the parts of the time-frequency plane for which the dip, strike and ellipticity are all consistent with Rayleigh-type behaviour (the masking functions are shown in Fig. 10). This flexibility in filter design is a major strength of the technique.

References

Jurkevics, A., 1988. Polarization analysis of three-component array data, Bull.

Seism. Soc. Am. **78**, 1725-1743.

Pinnegar, C.R., 2006. Polarization analysis and polarization filtering of three component signals with the time-frequency S-transform, Geophys. J. Int, in

press.

Stockwell, R.G., Mansinha, L. & Lowe, R.P., 1996. Localization of the complex spectrum: The S transform, IEEE Trans. Signal Process., **44**, 998-1001.